PHYSICAL REVIEW A **82**, 010901(R) (2010)

Thermal Casimir-Polder shifts in Rydberg atoms near metallic surfaces

J. A. Crosse,[1,*] Simen Å. Ellingsen,[2] Kate Clements,[1] Stefan Y. Buhmann,[1] and Stefan Scheel[1]

[1]*Quantum Optics and Laser Science, Blackett Laboratory, Imperial College London, Prince Consort Road, London SW7 2AZ, United Kingdom*

[2]*Department of Energy and Process Engineering, Norwegian University of Science and Technology, N-7491 Trondheim, Norway*

(Received 10 May 2010; published 8 July 2010)

The Casimir-Polder (CP) potential and transition rates of a Rydberg atom above a plane metal surface at finite temperature are discussed. As an example, the CP potential and transition rates of a rubidium atom above a copper surface at 300 K are computed. Close to the surface we show that the quadrupole correction to the force is significant and increases with increasing principal quantum number n. For both the CP potential and decay rates one finds that the dominant contribution comes from the longest wavelength transition and the potential is independent of temperature. We provide explicit scaling laws for potential and decay rates as functions of atom-surface distance and principal quantum number of the initial Rydberg state.

DOI: 10.1103/PhysRevA.82.010901 PACS number(s): 34.35.+a, 32.80.Ee, 42.50.Ct, 42.50.Nn

Rydberg atoms—atoms excited to large principal quantum numbers n—have attracted much attention in recent decades [1,2]. Aside from the inherent interest of studying such extreme states, the exaggerated properties of these highly excited atoms make them ideal for examining the properties of a variety of systems that would be awkward to probe by other means. The large cross sections and weakly bound outer electrons associated with Rydberg atoms make them extremely sensitive to small-scale perturbations and dispersion potentials, such as the van der Waals (vdW) and Casimir–Polder (CP) potentials [3].

For example, the strong scaling of the free-space vdW potential between two Rydberg atoms with n ($\propto n^{11}$) leads to the Rydberg blockade mechanism which has been put forward as a candidate for implementing controlled gate operations between isolated atoms [4,5]. The effect relies on the massive level shift that one Rydberg atom experiences in close proximity to another.

Level shifts of similar origin arise if the atoms are brought into the vicinity of a macroscopic body. With the increasing ability to trap and manipulate atoms close to macroscopic bodies, the effects of these surface (CP) potentials have become a subject of great interest. Applications range from novel atom trapping methods [6] to atom chip physics [7]. Thus, it is of both fundamental and practical interest to understand the interplay between atoms in highly excited states and field fluctuations emanating from macroscopic bodies.

In this Rapid Communication we provide evidence that dispersion forces have a sizable effect on the energy levels of highly excited Rydberg atoms when brought close to metallic surfaces, with shifts on the order of several GHz expected at micrometer distances. Due to the large atom size, next-to-leading order terms in the multipole expansion of the radiation field give additional contributions in the MHz range. Despite the existence of large numbers of thermal photons at 300 K at the relevant atomic transition frequencies, the level shifts are in fact temperature independent [8].

For a given atom-field coupling $\hat{H}_{\rm int}$, the CP potential for an atom in state $|n\rangle$ and the radiation field in state $|q\rangle$ is given by the position-dependent part of the energy shift which, to second order in perturbation theory, reads

$$\delta E_n = \langle n,q|\hat{H}_{\rm int}|n,q\rangle + \sum_{n',q'\neq n,q} \frac{|\langle n,q|\hat{H}_{\rm int}|n',q'\rangle|^2}{E_{n+q}-E_{n'+q'}}, \quad (1)$$

where E_{n+q} are the unperturbed energy eigenvalues of the atom-field system. In the long-wavelength approximation, the electric field couples to the atomic dipole moment $\hat{\mathbf{d}}$ via the interaction Hamiltonian,

$$\hat{H}_{\rm int} = -\hat{\mathbf{d}}\cdot\hat{\mathbf{E}}(\mathbf{r}_A), \quad (2)$$

with the electric field given in terms of the classical Green tensor (for a recent review see, e.g., [9]),

$$\hat{\mathbf{E}}(\mathbf{r}) = \sum_{\lambda=e,m}\int d^3r'\int d\omega\, \boldsymbol{G}_\lambda(\mathbf{r},\mathbf{r}',\omega)\cdot\hat{\mathbf{f}}_\lambda(\mathbf{r}',\omega) + \text{h.c.}, \quad (3)$$

with

$$\boldsymbol{G}_e(\mathbf{r},\mathbf{r}',\omega) = i\frac{\omega^2}{c^2}\sqrt{\frac{\hbar}{\pi\varepsilon_0}\text{Im}\varepsilon(\mathbf{r}',\omega)}\boldsymbol{G}(\mathbf{r},\mathbf{r}',\omega), \quad (4)$$

$$\boldsymbol{G}_m(\mathbf{r},\mathbf{r}',\omega) = -i\frac{\omega}{c}\sqrt{\frac{\hbar}{\pi\varepsilon_0}\frac{\text{Im}\mu(\mathbf{r}',\omega)}{|\mu(\mathbf{r}',\omega)|^2}}[\boldsymbol{G}(\mathbf{r},\mathbf{r}',\omega)\times\overleftarrow{\nabla}']. \quad (5)$$

The Green tensor $\boldsymbol{G}(\mathbf{r},\mathbf{r}',\omega)$ solves the Helmholtz equation for a point source and contains all the information about the geometry of the system. The bosonic vector fields $\hat{\mathbf{f}}_\lambda(\mathbf{r},\omega)$ describe collective excitations of the electromagnetic field and the linearly absorbing dielectric matter.

The CP potential at temperature T acting on an atom in state $|n\rangle$ via a dipole interaction (2) is given by [10]

$$\begin{aligned} U_{\rm CP}^{\rm dip}(\mathbf{r}_A) &= \mu_0 k_B T {\sum_{j=0}^{\infty}}' \xi_j^2 \left[\boldsymbol{\alpha}(i\xi_j)\bullet\boldsymbol{G}^{(1)}(\mathbf{r}_A,\mathbf{r}_A,i\xi_j)\right] \\ &\quad + \mu_0\sum_{k\neq n}\omega_{kn}^2 n(\omega_{kn})(\mathbf{d}_{nk}\otimes\mathbf{d}_{kn})\bullet\text{Re}\boldsymbol{G}^{(1)}(\mathbf{r}_A,\mathbf{r}_A,\omega_{kn}), \end{aligned} \quad (6)$$

where $\bullet$ denotes the Frobenius inner product ($\boldsymbol{A}\bullet\boldsymbol{B} = \sum_{i_1\ldots i_k} A_{i_1\ldots i_k}B_{i_1\ldots i_k}$) and the primed summation means that

*jac00@imperial.ac.uk

the term with $j = 0$ contributes only with half-weight. Here $\boldsymbol{G}^{(1)}(\mathbf{r}_A,\mathbf{r}_A,\omega)$ is the scattering part of the Green tensor. The atomic polarizability is defined as

$$\boldsymbol{\alpha}(\omega) = \left[\frac{1}{\hbar}\sum_{k\neq n}\frac{\mathbf{d}_{nk}\otimes\mathbf{d}_{kn}}{(\omega_{kn}+\omega)} + \frac{\mathbf{d}_{nk}\otimes\mathbf{d}_{kn}}{(\omega_{kn}-\omega)}\right], \tag{7}$$

with $\omega_{kn} = (E_k - E_n)/\hbar$ denoting the atomic transition frequencies. The frequencies $\xi_j = 2\pi k_B T j/\hbar$, $j \in \mathbb{N}$ are the Matsubara frequencies and $n(\omega) = [e^{\hbar\omega/k_B T} - 1]^{-1}$ is the thermal photon number distribution.

The reflective part of the scattering Green tensor of an infinitely extended planar metal that fills the lower half-space $z < 0$ is given by [11]

$$\boldsymbol{G}^{(1)}(\mathbf{r},\mathbf{r}',\omega) = \int \frac{d^2k_\parallel}{(2\pi)^2}\boldsymbol{R}(\mathbf{k}_\parallel,z,z',\omega)e^{i\mathbf{k}_\parallel\cdot(\mathbf{r}_\parallel-\mathbf{r}'_\parallel)}, \tag{8}$$

with $\mathbf{r}_\parallel = (x,y,0)$, $\mathbf{k}_\parallel = (k_x,k_y,0)$, and $k_\parallel = |\mathbf{k}_\parallel|$. The reflection tensor $\boldsymbol{R}(\mathbf{k}_\parallel,z,z',\omega)$ has the form,

$$\boldsymbol{R}(\mathbf{k}_\parallel,z,z',\omega) = \frac{-i}{8\pi^2\beta_+}\sum_{\sigma=s,p} r_\sigma e^{i\beta_+(z+z')}\mathbf{e}_\sigma^+\otimes\mathbf{e}_\sigma^-. \tag{9}$$

Here, the unit vectors for s-polarized and p-polarized waves are $\mathbf{e}_s^\pm = \mathbf{e}_{k_\parallel}\times\mathbf{e}_z$ and $\mathbf{e}_p^\pm = (k_\parallel\mathbf{e}_z \mp \beta_+\mathbf{e}_{k_\parallel})/q$. The functions $r_s = [\varepsilon(\omega)\beta_+ - \beta_-]/[\varepsilon(\omega)\beta_+ + \beta_-]$ and $r_p = [\beta_+ - \beta_-]/[\beta_+ + \beta_-]$ are the usual Fresnel reflection coefficients for those waves with wave numbers $\beta_- = \sqrt{q^2\varepsilon(\omega) - k_\parallel^2}$ and $\beta_+ = \sqrt{q^2 - k_\parallel^2}$, and $q = \omega/c$. The permittivity of the metal surface is modeled by the Drude relation, $\varepsilon(\omega) = 1 - \omega_p/\omega(\omega + i\gamma)$, where ω_p and γ are the plasma frequency and the relaxation rate of the metal, respectively. Magnetic effects will be neglected.

Matrix elements of the dipole operator $\hat{\mathbf{d}} = e\hat{\mathbf{r}} = e\hat{r}\mathbf{e}_r$ for the transition between two electronic states $|n,l,j,m\rangle$ (n, principal quantum number; l,j,m, quantum numbers for orbital and total angular momentum and z component of the latter) and $|n',l',j',m'\rangle$ factor into a radial and an angular part according to

$$\langle n',l',j,m'|\hat{\mathbf{d}}|n,l,j,m\rangle = e\langle R_{n',l',j'}|\hat{r}|R_{n,l,j}\rangle\langle l'j'm'|\mathbf{e}_r|ljm\rangle, \tag{10}$$

where $|R_{n,l,j}\rangle$ are the radial wave functions. The radial matrix elements are computed numerically using the Numerov method [12,13] in which the suitably scaled radial Schrödinger equation is integrated inward until an inner cutoff point (commonly the radius of the rump ion). The eigenenergies are computed as $E_{n,l,j} = -\mathcal{R}/n^{*2}$ ($\mathcal{R}$ is the Rydberg constant) where $n^* = n - \delta_{n,l,j}$ is the effective quantum number and $\delta_{n,l,j}$ the quantum defect [14] whose values are tabulated in the literature [15].

To evaluate the angular part, we first convert from the jm basis to a $m_l m_s$ basis (m_l, m_s are the z components of orbital angular momentum and spin) by summing over the relevant Clebsch-Gordan coefficients,

$$\langle l'j'm'|\mathbf{e}_r|ljm\rangle = \sum_{\substack{m_l m'_l\\ m_s}} C^{j,l,1/2}_{m,m_l,m_s} C^{j',l',1/2}_{m',m'_l,m_s}\langle Y_{l',m'_l}|\mathbf{e}_r|Y_{l,m_l}\rangle, \tag{11}$$

with the orbital-angular momentum eigenstates $|Y_{l,m_l}\rangle$ being spherical harmonics. Matrix elements in the $m_l m_s$ basis are computed by rewriting the radial unit vector in terms of spherical harmonics [$Y_{lm} \equiv Y_{lm}(\vartheta,\varphi)$],

$$\mathbf{e}_r = \sqrt{\frac{2\pi}{3}}\begin{pmatrix} Y_{1,-1} - Y_{1,1}\\ i(Y_{1,-1} + Y_{1,1})\\ \sqrt{2}Y_{1,0}\end{pmatrix}, \tag{12}$$

and using the integral relation [$d\Omega \equiv \sin\vartheta\, d\vartheta\, d\varphi$],

$$\int d\Omega\, Y_{l_1,m_1}Y_{l_2,m_2}Y_{l_3,m_3} = \sqrt{\frac{1}{4\pi}\prod_{v=1}^{3}(2l_v+1)}\begin{pmatrix} l_1 & l_2 & l_3\\ 0 & 0 & 0\end{pmatrix}\begin{pmatrix} l_1 & l_2 & l_3\\ m_{l_1} & m_{l_2} & m_{l_3}\end{pmatrix} \tag{13}$$

that expresses the angular integral over three spherical harmonics in terms of Wigner $3j$ symbols.

When Rydberg atoms are held sufficiently close to a surface, their effective radius $\langle r\rangle \simeq a_0 n^2$ (a_0 is the Bohr radius) can be on the order of micrometers and therefore a significant fraction of the surface distance. The dipole approximation is then no longer appropriate. In other words, the atom cannot be viewed as a point-like particle, and its non-negligible size requires the inclusion of contributions from higher-order multipoles. This correction can be found via a similar method as described previously, with the dipole interaction Hamiltonian replaced by the quadrupole interaction Hamiltonian [16],

$$\hat{H}_{\rm int} = -\hat{\mathbf{Q}}\bullet[\nabla\otimes\hat{\mathbf{E}}(\mathbf{r}_A)]. \tag{14}$$

In close analogy to the dipole case the CP potential for a quadrupole interaction is found to be

$$U_{\rm CP}^{\rm quad}(\mathbf{r}_A) = \mu_0 k_B T\sum_{j=0}^{\infty}{}'\xi_j^2\boldsymbol{\alpha}^{(4)}(i\xi_j) \bullet[\nabla\otimes\boldsymbol{G}(\mathbf{r}_A,\mathbf{r}_A,i\xi_j)\otimes\overleftarrow{\nabla}] + \mu_0\sum_{k\neq n}\omega_{kn}^2 n(\omega_{kn}) \times(\mathbf{Q}_{nk}\otimes\mathbf{Q}_{kn})\bullet[\nabla\otimes{\rm Re}\boldsymbol{G}(\mathbf{r}_A,\mathbf{r}_A,\omega_{kn})\otimes\overleftarrow{\nabla}], \tag{15}$$

with the quadrupole moment operator $\hat{\mathbf{Q}} = e(\hat{\mathbf{r}}\otimes\hat{\mathbf{r}})/2$ and the atomic quadrupole polarizability defined as

$$\boldsymbol{\alpha}^{(4)}(\omega) = \frac{1}{\hbar}\sum_{k\neq n}\left[\frac{\mathbf{Q}_{nk}\otimes\mathbf{Q}_{kn}}{(\omega_{kn}+\omega)} + \frac{\mathbf{Q}_{nk}\otimes\mathbf{Q}_{kn}}{(\omega_{kn}-\omega)}\right]. \tag{16}$$

The matrix elements for the quadrupole transitions can again be evaluated by factoring $\hat{\mathbf{Q}} = (e/2)\hat{r}^2\mathbf{e}_r\otimes\mathbf{e}_r$ and computing the matrix elements between the radial and angular parts of the wave functions separately. Evaluation of the radial integral is again performed numerically. The tensor product of unit vectors in spherical harmonic form reads $\mathbf{e}_r\otimes\mathbf{e}_r = \sqrt{\frac{2\pi}{15}}{\rm A}$ with

$$A_{\substack{xx\\yy}} = \pm Y_{2,-2} \pm Y_{2,2} - \sqrt{\frac{2}{3}}Y_{2,0} + \sqrt{\frac{10}{3}}Y_{0,0}, \tag{17a}$$

$$A_{xy} = A_{yx} = i(Y_{2,-2} - Y_{2,2}), \tag{17b}$$

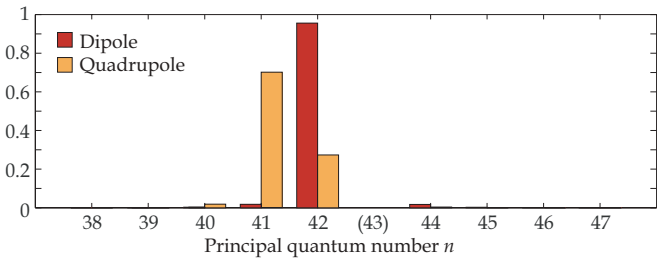

FIG. 1. (Color online) Relative contributions from different transitions to the CP dipole and quadrupole level shift of the state $43s$ of ^{87}Rb.

$$A_{xz} = A_{zx} = Y_{2,-1} - Y_{2,1}, \tag{17c}$$

$$A_{yz} = A_{zy} = i(Y_{2,-1} + Y_{2,1}), \tag{17d}$$

$$A_{zz} = \sqrt{\frac{8}{3}}Y_{2,0} + \sqrt{\frac{10}{3}}Y_{0,0}. \tag{17e}$$

The angular matrix elements can then be evaluated using Eq. (13).

As can be seen from Eqs. (6) and (15), the CP potential is comprised of a pair of sums, one over the Matsubara frequencies and one over all available atomic transitions. It turns out, however, that due to the finite-temperature environment only a limited number of dipole and quadrupole transitions contribute significantly to the total level shift. This effect is depicted in Fig. 1, where we show the relative contributions of the dipole transitions $43s \rightarrow np$ and quadrupole transitions $43s \rightarrow nd$ to the total level shift of the $43s$ state of ^{87}Rb. Note that the dominant transitions are different for dipole and quadrupole shifts. This is due to the differing quantum defects for the respective target p and d states. Moreover, for each of these individual (long-wavelength) transitions the first term in the Matsubara sum (with $j = 0$) dominates at the micrometer atom-surface distances envisaged here, and all other terms can be safely neglected. Remarkably, we observe that the CP potential is independent of temperature from $T = 0 - 300$ K and beyond. As was recently shown [8], this is due to the dominance of contributions from transitions whose wavelengths far exceed atom-surface separations.

Figure 2(a) shows the total CP potential (and hence level shifts) $U_{\rm CP} = U_{\rm CP}^{\rm dip} + U_{\rm CP}^{\rm quad}$ for various ns states (with $n =$ 32,43,54) of ^{87}Rb near a copper surface at 300 K. As we are not interested in a particular transition channel, the weighted sum over all possible final states has been taken.

One observes that for very small (yet experimentally achievable and indeed desirable) distances of less than 2 μm the expected level shifts rapidly grow to GHz sizes. At these distances, we also observe significant deviations of the total shift from the dipole contribution (6) alone due to the increasingly important quadrupole shifts [Eq. (15)] which themselves can be as large as several MHz [inset in Fig. 2(a)].

Related to the energy level shift is a line broadening effect (i.e., an increased rate of spontaneous decay due to strong nonradiative processes) as the atom approaches the surface [9,16]. This strongly enhanced body-induced spontaneous decay partially counteracts the expected increase in lifetime as a function of the principal quantum number n in free space ($\Gamma_0 \propto n^{-3}$) [1].

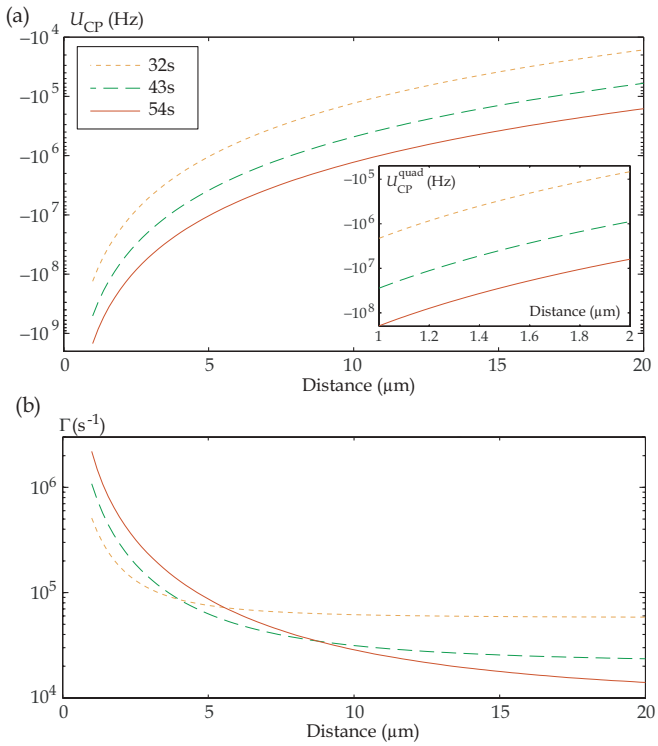

FIG. 2. (Color online) (a) Casimir-Polder level shifts of the states $32s$ (dotted line), $43s$ (dashed line), and $54s$ (solid line) of ^{87}Rb near a copper surface at 300 K; total shift and quadrupole contribution alone (inset). (b) Spontaneous decay rate near a copper surface at 300 K for the initial states $32s$ (dotted line), $43s$ (dashed line), and $54s$ (solid line) of ^{87}Rb.

In Fig. 2(b) we show the total decay rates of the Rydberg states ns ($n = 32,43,54$) of ^{87}Rb as a function of atom-surface distance. The body-induced decay rates for electric dipole and quadrupole transitions are calculated from Ref. [16] as [$\Gamma_{nk} = \Gamma_{nk}^{\rm dip} + \Gamma_{nk}^{\rm quad}$]

$$\Gamma_{nk}^{\rm dip}(\mathbf{r}_A) = \frac{\omega_{nk}^2}{\hbar\varepsilon_0 c^2}(\mathbf{d}_{nk} \otimes \mathbf{d}_{kn}) \bullet \mathrm{Im}\, \boldsymbol{G}(\mathbf{r}_A, \mathbf{r}_A, |\omega_{nk}|) \times \{\Theta(\omega_{nk})[n(\omega_{nk}) + 1] + \Theta(\omega_{kn})n(\omega_{kn})\}, \tag{18}$$

$$\Gamma_{nk}^{\rm quad}(\mathbf{r}_A) = \frac{\omega_{nk}^2}{\hbar\varepsilon_0 c^2}(\mathbf{Q}_{nk} \otimes \mathbf{Q}_{kn}) \bullet [\nabla \otimes \mathrm{Im}\, \boldsymbol{G}(\mathbf{r}_A, \mathbf{r}_A, |\omega_{nk}|) \otimes \overleftarrow{\nabla}] \times \{\Theta(\omega_{nk})[n(\omega_{nk}) + 1] + \Theta(\omega_{kn})n(\omega_{kn})\}. \tag{19}$$

Note that, unlike the CP potential, the decay rates are always temperature dependent. One observes a strong increase of the decay rates near the surface ($z \lesssim 10$ μm) which becomes more pronounced for states with higher principal quantum number n. This translates into a relative line broadening of more than three orders of magnitude that potentially limits trapping and manipulation times of high-lying states near surfaces. For larger distances ($z \gtrsim 15$ μm) the rates quickly approach their free-space values and show the expected suppression with increasing n.

Finally, we will briefly consider how the CP potential and transition rates scale with atom-surface distance z and the principal quantum number n. For metal surfaces, the reflection

coefficients are nearly independent of ω at infrared frequencies and below. In the low-temperature limit, when the thermal photon number is negligible, there is no ω dependence for either the CP potential or the transition rates. The dipole and quadrupole moments for the dominant $ns \to (n-1)p$ and $ns \to (n-1)d$ transitions scale as n^2 and n^4, respectively, for large n. In the nonretarded limit (valid for surface distances beyond even 100 μm), the body-induced rates and the CP potential scale as z^{-3} and z^{-5} for the dipole and quadrupole contributions, respectively [16]. Combining these results leads to a scaling behavior of

$$\left|U_{\mathrm{CP}}^{\mathrm{dip}}\right|, \quad \Gamma_{nk}^{\mathrm{dip}} \propto \frac{n^4}{z^3}, \quad \left|U_{\mathrm{CP}}^{\mathrm{quad}}\right|, \quad \Gamma_{nk}^{\mathrm{quad}} \propto \frac{n^8}{z^5}, \tag{20}$$

for the dipole and quadrupole components of the CP potential U_{CP} and the decay rate Γ_{nk}.

In the high-temperature limit, the scaling of the CP shifts remains the same due to the temperature independence demonstrated in Ref. [8], whereas the transition rates become proportional to the mean photon number $n(\omega) \approx k_B T/(\hbar\omega)$. For the dominant dipole and quadrupole transitions (Fig. 1), one finds $\omega \propto n^{-3}$, and the transition rates scale as $\Gamma_{nk}^{\mathrm{dip}} \propto n^7/z^3$ and $\Gamma_{nk}^{\mathrm{quad}} \propto n^{11}/z^5$, respectively.

We have shown in this Rapid Communication that the interaction between highly excited atoms and macroscopic surfaces leads to energy level shifts that can be as large as several GHz. This implies that any scheme that relies on the manipulation of (trapped) Rydberg atoms near surfaces has to account for this major adjustment. Moreover, some of the advantages of using highly excited Rydberg atoms, in particular their rapidly decreasing Einstein coefficients with increasing principal quantum number n, are counteracted by the atom-surface interactions.

ACKNOWLEDGMENTS

We thank D. Cano and J. Fortágh for helpful discussions. This work was supported by the UK Engineering and Physical Sciences Research Council. Support from the European Science Foundation (ESF) within the activity "New Trends and Applications of the Casimir Effect" is gratefully acknowledged.

[1] T. F. Gallagher, *Rydberg Atoms* (Cambridge University Press, Cambridge, 1994).
[2] T. Nakajima, P. Lambropoulos, and H. Walther, Phys. Rev. A **56**, 5100 (1997).
[3] H. B. G. Casimir and D. Polder, Phys. Rev. **73**, 360 (1948).
[4] M. D. Lukin *et al.*, Phys. Rev. Lett. **87**, 037901 (2001).
[5] H. Kübler *et al.*, Nature Photonics **4**, 112 (2010).
[6] H. Bender, P. Courteille, C. Zimmermann, and S. Slama, Appl. Phys. B **96**, 275 (2009).
[7] J. Fortágh and C. Zimmermann, Rev. Mod. Phys. **79**, 235 (2007).
[8] S. Å. Ellingsen, S. Y. Buhmann, and S. Scheel, Phys. Rev. Lett. **104**, 223003 (2010).
[9] S. Scheel and S. Y. Buhmann, Acta Phys. Slov. **58**, 675 (2008).
[10] S. Y. Buhmann and S. Scheel, Phys. Rev. Lett. **100**, 253201 (2008).
[11] W. C. Chew, *Waves and Fields in Inhomogeneous Media* (IEEE Press, New York, 1995).
[12] J. M. Blatt, J. Comput. Phys. **1**, 382 (1967).
[13] S. A. Bhatti, C. L. Cromer, and W. E. Cooke, Phys. Rev. A **24**, 161 (1981).
[14] M. Seaton, Rep. Prog. Phys. **46**, 167 (1993).
[15] W. Li, I. Mourachko, M. W. Noel, and T. F. Gallagher, Phys. Rev. A **67**, 052502 (2003); C.-J. Lorenzen and K. Niemax, Phys. Scr. **27**, 300 (1983).
[16] J. A. Crosse and S. Scheel, Phys. Rev. A **79**, 062902 (2009).